Composites Part C: Open Access 17 (2025) 100605

Contents lists available at ScienceDirect

Composites Part C: Open Access

journal homepage: www.sciencedirect.com/journal/composites-part-c-open-access

Degradation behaviour and damage mechanisms of carbon fibre reinforced polymer composite laminates subjected to laser irradiation

Patrick K. Kamlade [a,1], Jojibabu Panta [a,†], Max Mammone [a], Richard (Chunhui) Yang [a], Richard P. Mildren [b], John Wang [c], Matthew Ibrahim [c], Rodney Thomson [d], Y.X. Zhang [a,e,*]

[a] Centre for Advanced Manufacturing Technology, School of Engineering, Design and Built Environment, Western Sydney University, Locked Bag 1797, Penrith, NSW 2751, Australia
[b] MQ Photonics Research Centre, School of Mathematical and Physical Sciences, Macquarie University, Macquarie Park, NSW 2109, Australia
[c] Platforms Division, Defence Science and Technology Group, Melbourne, VIC 3207, Australia
[d] Advanced Composite Structures Australia Pty Ltd, 19 Rocklea Drive, Port Melbourne 3207, Australia
[e] School of Mechanical and Mechatronic Engineering, University of Technology Sydney, Ultimo, NSW 2007, Australia

ARTICLE INFO

Keywords:
Carbon fibre reinforced polymer (CFRP)
Damage
Degradation behaviour
Laser irradiation
Material characterisation
Thermal stability

ABSTRACT

This study presents a comprehensive and insightful investigation into the thermal degradation and damage mechanisms of carbon fibre reinforced polymer (CFRP) composite laminates exposed to continuous wave laser irradiation with a Gaussian beam profile. The effects of laser power, beam diameter, and exposure time were explored to reflect practical scenarios such as material processing, maintenance, and damage assessment. Thermogravimetric analysis (TGA) was first carried out in both nitrogen and air environments to understand the thermal stability and degradation behaviour of the CFRP material. Initial laser tests were conducted at 30 W and 40 W using a beam diameter of 3.46 mm to assess early-stage damage. These results informed a more intensive study using a higher laser power of 98 W with beam diameters of 3.18 mm and 5.70 mm, where specimens were irradiated until complete perforation. Thermal imaging was used to monitor surface temperature evolution on both front and back sides during irradiation. For the 98 W cases, the larger beam diameter required a 53 % longer exposure time to achieve perforation, highlighting the role of power density in damage progression. Post-irradiation analysis using scanning electron microscopy (SEM), ultrasonic C-scans, and micro-focused X-ray computed tomography (micro-CT) revealed fibre sublimation, matrix decomposition, cone-shaped perforations, and interlaminar cracking. The results provide valuable insights into how CFRP materials respond to high-intensity laser exposure and can support the development of strategies to mitigate damage and improve structural performance in real-world applications.

1. Introduction

Carbon fibre reinforced polymers (CFRPs) are widely used in various aerospace structures due to their outstanding mechanical characteristics including high strength–to–weight ratio, excellent corrosion resistance, and good formability [1–3]. Composite skin-stiffened panels made of CFRP are considered essential components and are extensively employed in both primary and secondary load-bearing aircraft structures because of their higher load-carrying efficiency [4–6]. However, their temperature operational range is lower than that of traditionally used metal structures.

High-energy lasers can rapidly vaporise materials through opto-thermal transformation [7–9]. Pulsed lasers have been extensively used in material processing for several decades because of their highly localised heat input and minimal distortion [10–12]. Continuous wave (CW) lasers are more powerful due to their higher average power output and can cause material damage quickly due to thermal effects [13–15], but very limited studies have been reported. The advancement of increasingly powerful CW laser systems with large laser spots has highlighted the need for effective anti-laser ablation measures [16]. The interaction between lasers and materials holds significance in fundamental science, material processing and the manufacturing industry

* Corresponding author at: School of Mechanical and Mechatronic Engineering, University of Technology Sydney, Ultimo, NSW 2007, Australia.
E-mail address: sarah.zhang@uts.edu.au (Y.X. Zhang).
[1] Joint first authors.

https://doi.org/10.1016/j.jcomc.2025.100605

Available online 10 May 2025

[17–20]. In examining the fundamental aspect of laser interaction with carbon-based composites, one can view the laser beam as traversing from the surface to an intermediate region through multiple absorption and scattering events. Absorption of the laser irradiation within the CFRP matrix and fibres results in intense heating and is the primary mechanism leading to the destruction of CFRP by a laser beam [21,22]. A laser power density of 10 W/mm^2 can potentially burn carbon-based composite materials completely, with local temperatures reaching as high as 3250 °C [23]. Consequently, lasers are viewed as an effective tool for degrading composite materials.

This phenomena of laser-induced damage to CFRPs are applicable to various industrial environments [16,24]. This includes repair and maintenance depots, where laser-based technologies are used for cleaning, cutting, or processing composite materials. These processes can generate high thermal loads on CFRP components, potentially leading to localised damage. Additionally, lasers may be used in composite manufacturing processes, where exposure to high-power lasers during automated cutting or material processing operations can compromise the integrity of the material. Such situations highlight the importance of understanding the behaviour of CFRPs under laser exposure, not only for material processing and manufacturing, but also for the development of protective measures in aerospace and industrial applications.

The extent and nature of damage by lasers to CFRPs depends on many parameters including the laser power, beam diameter, exposure duration, the inherent properties of the composites, and the medium the laser beam travels through to reach the composite [24–28]. As a laser beam travels through the atmosphere, its intensity can be reduced through particles within it that absorb, scatter and diffract its energy [16,24]. These effects can be negated within a controlled laboratory environment. Upon laser irradiation striking a CFRP material, absorption of the laser's energy initially results in the CFRP's matrix component melting or evaporating due to the evaporation temperature of polymers being hundreds of degrees lower than that of carbon fibres. As the temperature increases, thermal stresses within CFRP occur, which results in cracks and internal delamination within the material [29]. Subsequently, there is a continual outflow of material from the surface as the matrix component degrades. The heat generated as the CFRP absorbs the laser irradiation travels primarily along the more thermally conductive fibres, leading to fibre-matrix separation and subsequent reduction in the mechanical properties of the material [30]. The evaporation of the matrix component throughout each of the aforementioned processes can lead to the carbon fibres being directly exposed to the laser beam irradiation resulting in further damage to the CFRP [31].

Wolfrum et al. [32] studied the effects of CW laser irradiation on CFRP panels of varying thicknesses, revealing a linear relationship between laser energy, perforation time, and the size of the damaged volume. Their findings indicated that higher laser energy reduced residual compressive strength and resulted in thermal damage extending beyond the immediate laser spot. Zhang et al. [33] investigated the ablation behaviour of CFRP laminates under different laser power densities, noting that higher power densities led to increased heat affected zone (HAZ) size, crater depth, and ablation rates. Their work presented how laser power impacted the extent and distribution of thermal damage within the material. Liu et al. [34] studied interlaminar damage in CFRP composites by examining the effects of CW laser irradiation. Their research highlighted the relationship between laser parameters and interface cracking patterns, offering insights into the damage behaviour. Existing literature on CFRPs typically examined the surface damage and structural weakening caused by laser exposure, but detailed analyses of the internal microstructural changes and thermal effects are relatively less [27,32–34].

Key gaps in the current literature are the lack of detailed and intensive studies on the effect of prolonged exposure times on CFRP laminates under varying heat fluxes and the effect of varying laser beam diameters on CFRP laminates under the same laser power. While previous research has predominantly focused on general ablation mechanisms, the influence of changing power density, specifically by altering the beam diameter, on temperature distribution, damage progression, and perforation times has not been thoroughly explored. This study addresses these gaps by investigating how varying heat fluxes influence thermal degradation and material integrity at a microstructural level over extended exposure times.

In this study, the effects of laser irradiation on EA9396-based CFRP, manufactured using the wet lay-up method, were investigated. The wet lay-up method offers several advantages: (1) it allows for easy evaluation of matrix properties separately, (2) it provides a foundation for further research on how additives such as nanoparticles can enhance laminate resistance to laser damage, and (3) EA9396 resin offers improved adhesive strength at elevated temperatures [35,36]. CW laser irradiation was applied to the CFRP samples using a Gaussian beam profile. Initial laser tests were conducted at power outputs of 30 W and 40 W using a CW laser with a Gaussian beam profile to evaluate the preliminary thermal response and damage behaviour of the CFRP specimens. These relatively low-power tests provided foundational insight into the onset of thermal degradation and surface effects under prolonged irradiation. The findings informed a more detailed investigation involving a higher laser power of 98 W, where two different beam diameters were employed to assess the influence of laser intensity. The thermal stability of the CFRP material was first evaluated using thermogravimetric analysis (TGA) in both nitrogen and air environments. During laser exposure, temperature distributions were captured on the front and rear surfaces using high-resolution thermal imaging cameras. Post-irradiation characterisation was performed using optical microscopy, scanning electron microscopy (SEM), X-ray micro-computed tomography (micro-CT), and ultrasonic C-scans to assess surface damage and internal structural changes. The combination of these advanced techniques enabled a comprehensive understanding of the thermal and structural response of CFRP under varying laser irradiation conditions.

2. Experimental programs

2.1. Preparation of CFRP laminate specimens

The fabrication of the CFRP laminate specimens involved the use of an aerospace-grade epoxy system (LOCTITE EA 9396, Aerospace Materials, Australia) and a 3k carbon plain-weave fabric weighing 195 gsm (SP Systems, United Kingdom). The manufacturing process used a wet lay-up technique, with an initial fibre-to-resin ratio of 1:1 Parts-By-Weight (PBW) to fully wet out the carbon fibres while achieving a high fibre content. The nominal void and fibre volume fractions of the CFRP were determined through acid digestion to be 14 vol. % and 49 vol. %, respectively. The laminates were comprised of 16 plies of the plain weave fabric, each stacked with the warp ply directions aligned parallel. After lay-up and vacuum bagging, a vacuum pressure ranging from −70 to −80 kPa was applied during the curing process, carried out for 24 h at 25 °C, followed by a 4-hour post-cure cycle at 80 °C. A computer numerical control (CNC) milling machine (COMPCUT) was used to extract the specimens for laser irradiation with dimensions of 50 × 50 × ~ 4.6 mm^3.

2.2. Laser testing of CFRP laminate specimens

Laser irradiation was conducted using CW fibre lasers operating in the near-infrared wavelength range that consisted of a linearly polarised beam and a Gaussian spatial profile. Each of the laser beam diameters listed are measured using the D4σ method with a camera beam profiler.

For the 30 W and 40 W exposures, a 1064 nm distributed feedback seed laser (Toptica DL DFB BFY 1064) was amplified using a commercial ytterbium-doped fibre amplifier (PreciLasers YFA-1064–80-CW). The beam was directed over a 1 m path using high-reflectivity mirrors to a final measured spot diameter of 3.46 mm. The resulting peak intensities

were 6.37 W/mm² for 30 W and 8.45 W/mm² for 40 W.

For the 98 W exposures, a 1045 nm seed laser (Innolume 1045.3-PM-25) was spectrally broadened to a full width at half-maximum bandwidth of 4 GHz using an electro-optic modulator (ixBlue) driven by an amplified additive white Gaussian noise source. The broadened output was then amplified through two ytterbium-doped fibre amplifier stages (Civil Laser YDFA-27-PM-B and FILASE 1040–1060 nm fibre amplifier). The beam was delivered over a 2.75 m path and shaped using lenses to obtain two different spot diameters: 3.18 mm and 5.70 mm, corresponding to peak intensities of 24.7 W/mm² and 7.68 W/mm², respectively.

The laser testing setup for low power and high power tests is illustrated in Fig. 1. CFRP specimens were mounted vertically and perpendicular to the incident laser beam using a fixed holder beneath an upward airflow extraction system. This setup ensured efficient removal of vaporised debris and minimised beam scatter during exposure. Perforation was monitored using a light meter that had a portion of the laser beam that passed through the CFRP specimen reflected to it via a glass plane. A beam sink was positioned behind the glass plane to absorb excess transmitted energy to prevent reflections and collateral damage.

Thermal measurements were obtained using calibrated infrared cameras. For the 30 W and 40 W tests, a Micro-Epsilon TIM 160 s (Germany) with a maximum measurable temperature of 900 °C (±2 %), was used to capture front surface temperature at 20 Hz, that was placed 200 mm from the target at a 30° viewing angle. For the 98 W tests, a FLIR T865 (USA) rated up to 2000 °C (±3 %), was used to record the front surface temperature at 30 Hz from a 250 mm distance and 20° angle viewing angle, while a Micro-Epsilon TIM 160 s camera measured the rear surface temperature at 20 Hz from a 270 mm distance and 60° viewing angle. All thermal cameras were set to record for an emissivity of 0.95 and an ambient temperature of 20 °C.

For the 30 W and 40 W conditions, samples were irradiated for up to 10 min to observe the progression of thermal degradation. For the 98 W tests, full perforation experiments were conducted first to characterise the maximum extent of damage, followed by partial exposure tests at one-quarter and one-half of the average perforation time. Four replicate tests were conducted under full perforation conditions, and three replicates for each partial exposure duration, ensuring repeatability in key response metrics such as perforation time, rear surface temperature rise, and mass loss.

2.3. Characterisation of laser damaged CFRP laminate specimens

The thermal degradation characteristics of the CFRP laminates were determined using a Netzsch STA 449C Jupiter TGA under nitrogen and air atmospheres at a flow rate of 25 mL/min. This method helps identify distinct phases of CFRP material decomposition. Air and nitrogen environments were used to observe differences in the degradation of the CFRP laminate in an oxidative and non-oxidative environment. The analysis involved 10 mg CFRP specimens placed in aluminium pans, following a constant heating rate of 10 °C/min from 25 °C to 900 °C.

Post-laser irradiation, the surface and subsurface of the CFRP specimens were examined using several characterisation techniques. Initial efforts focused on understanding the in-plane damage morphology, employing optical and SEM (Hitachi Flex 1000 II). The optical macroscopic images provided an overview of the damage boundary, while SEM images (at 5 kV) showed detailed insights into the extent of damage within individual phases (matrix and fibre).

For the specimens subjected to laser irradiation of 98 W, the following additional characterisation methods were also performed. The extent of internal damage suffered by the CFRP laminates during irradiation was determined via ultrasonic C-scanning. Irradiated specimens were immersed in a water bath and inspected in both reflection and transmission using an 11-axis mechanical raster ultrasonic system (TecScan Systems, Canada). The ultrasound was generated from a pulsed square-wave generator, resulting in a 5 MHz centre frequency in two Technisonic ISL-0504-HR 0.5 in diameter piezoelectric probes having a spherical focal length of 3 in., and electronically processed by the TecScan TecView2 data acquisition and analysis software. Scanning was performed in a mechanical raster at a spatial resolution of 0.5 mm in both lateral dimensions. Data was presented on a qualitised dB colour scale of reflected and transmitted sound, respectively.

For investigating subsurface damage of the laser-irradiated CFRP specimens, micro-CT (Xylon CT precision system, Germany) was employed. The resolution of the two-dimensional slices was set at 20 μm/pixel.

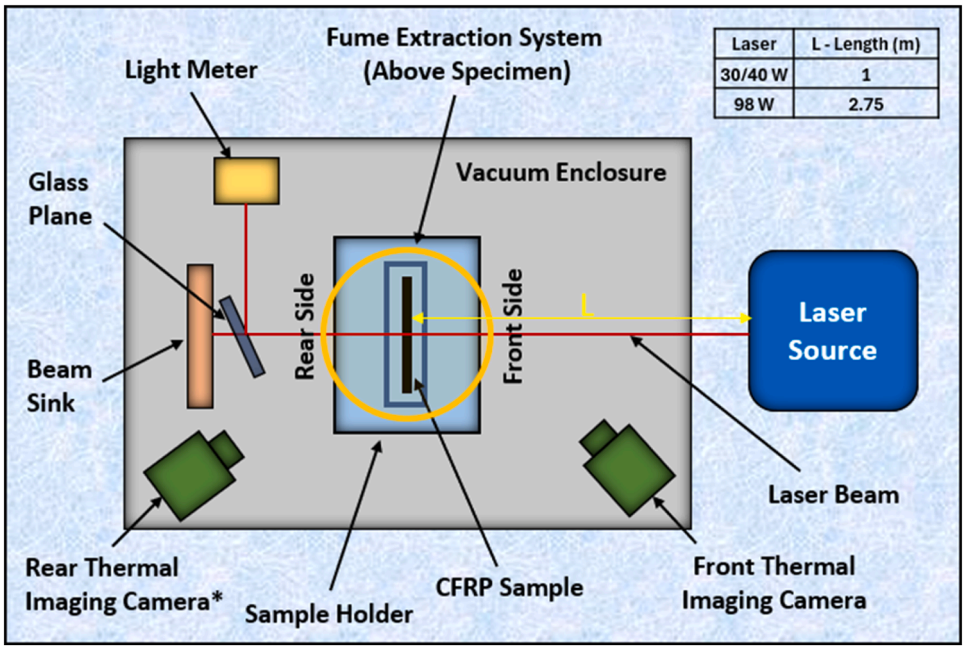

Fig. 1. Schematic of the experimental setup for laser irradiation of the CFRP specimens. The asterisk (*) denotes additional equipment used only for the setup with the 98 W laser tests.

3. Results and discussion

3.1. Thermal stability of the CFRP laminate specimens

Thermal characterisation studies were performed to observe the effect of the degradation behaviour of the CFRP laminates under elevated temperatures. TGA curves of CFRP under nitrogen and air atmosphere are illustrated in Fig. 2. In a nitrogen atmosphere, CFRP degradation commenced at approximately 350 °C, and the thermal degradation process unfolded as a single stage within the temperature range of 300–500 °C. The resulting final char at 900 °C amounted to approximately 52 %, primarily attributed to the degradation of the epoxy resin. On the other hand, the CFRP laminate exhibited distinct degradation patterns in air, manifesting in a three-step process occurring within specific temperature ranges: 250–450 °C, 500–650 °C, and 660–800 °C. Initially, the epoxy networks underwent a decomposition process, yielding a char and resulting in a 27 % mass loss. Subsequently, the char underwent oxidation, leading to complete volatilisation, including the release of gases including carbon monoxide (CO) and carbon dioxide (CO_2), marking the second stage with a 23 % mass loss. The third phase involved the oxidation and degradation of carbon fibres, attributed to the formation of CO and CO_2 during heating. Ultimately, at 800 °C, the carbon fibres were entirely oxidised into gases, resulting in 0 % char content in the CFRP [37].

3.2. Low power laser irradiation (30 W and 40 W): thermal behaviour and degradation characteristics

Initial CW laser tests using 30 W and 40 W powers with a fixed beam diameter of 3.46 mm were performed to examine the early-stage thermal response and degradation of CFRP laminates under localised heating. These tests provided critical insights into heat transfer, matrix decomposition, and damage progression under relatively moderate energy input, and were used to guide the design of the subsequent high-power laser testing.

Thermal imaging (Fig. 3) captured the surface temperature distribution during irradiation. In both cases, the maximum measurable temperature of 900 °C was reached almost immediately after the laser was turned on and remained at this limit throughout the 600 s exposure. The area subjected to temperatures above 150 °C was visibly larger for the 40 W condition, consistent with the higher power density applied. Temperature data collected from a fixed location near the beam centre Fig. S1 (supplementary information) showed rapid initial heating, associated with surface matrix pyrolysis, followed by a relatively stable plateau due to thermal equilibrium between the incident laser energy and the heat dissipation mechanisms.

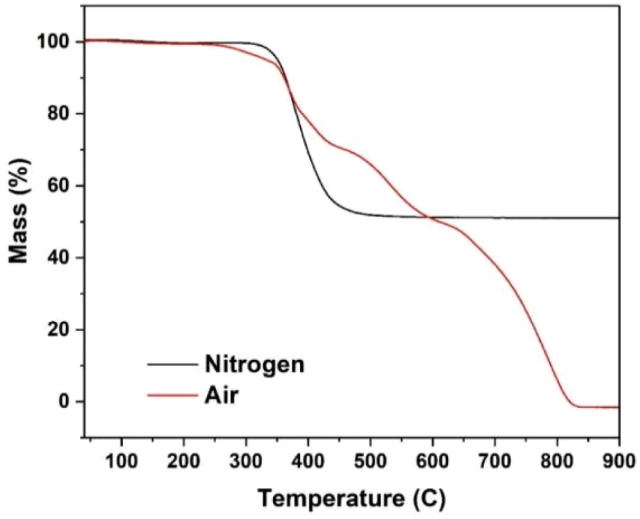

Fig. 2. TGA curves for the CFRP laminate in nitrogen and air atmospheres at a constant heating rate of 10 °C/min.

The macro-morphologies of the front surface following irradiation (Fig. 4) showed a well-defined circular damage region corresponding to the beam profile. More pronounced char and soot deposition was observed on the 40 W specimens, particularly towards the upper edge of the irradiated region, aligned with the direction of the airflow from the overhead extraction system. This suggests active transport of gaseous decomposition products during irradiation and surface re-deposition of carbonaceous material. The effect of increasing power was further evident in the measured mass loss. Over the 600 s exposure, the mass loss increased from 1.48 % for the 30 W specimen to 2.71 % for the 40 W specimen, reflecting a direct correlation with the increase in incident energy. This increase is attributed to enhanced matrix degradation and partial fibre damage under higher laser flux (6.37 W/mm^2 and 8.45 W/mm^2, respectively).

SEM images revealed matrix ablation, fibre-matrix debonding, and the onset of fibre degradation as shown in Fig. S2. The 30 W specimens primarily showed resin depletion and exposure of intact fibres, whereas the 40 W samples exhibited more extensive matrix degradation, surface pitting, and signs of local fibre damage. These results established key trends in temperature development, mass loss, and surface damage associated with relatively low-power laser irradiation. Importantly, they provided a baseline for understanding material response under controlled conditions, which informed the approach to higher-power testing. The observations from these initial tests were used to calibrate the exposure parameters and analytical techniques employed in the 98 W laser study, where more severe damage, internal delamination, and through-thickness failure mechanisms were expected due to the increased energy input and focused beam intensities.

3.3. Temperature distribution in the CFRP laminate during 98 W laser power irradiation

The temperature distribution in the CFRP specimens during laser irradiation was captured using front and back thermal imaging cameras. Figs. 5 and 6 show a series of images depicting the temperature distribution on the front and rear surfaces of CFRP specimens, respectively, when exposed to a laser power of 98 W and a beam diameter of 3.18 mm. The images are captured at different exposure times of 60, 156, 312 and 625 s after the onset of laser irradiation, with the perforation occurring at approximately 625 s.

On the front surface (Fig. 5a) at 60 s of exposure time, there is a clear observation of a yellow-hot centre with red-hot radiation fringes as the laser beam initiates heating. This heat begins to transfer to the rear surface of the specimen (Fig. 6a). Typically, the epoxy matrix within CFRP exhibits almost transparent qualities to light and the rapid conduction observed within the CFRP stems primarily from the carbon fibres. During this exposure time, the specimen catches fire as the epoxy reaches a sufficiently high temperature to combust, with flames initiating on the laminate surface. Subsequently, as depicted in Figs. 5b and 6b (at a quarter penetration time of 156 s), the higher temperature regions propagate further across the specimen. These radiations continue to spread, and the flames persist alongside steady yellow-hot radiation as the epoxy burn-off phase approaches its end and transitions to material degradation (Figs. 5b–d and 6b–d). This shift marks the onset of carbon fibre degradation. Figs. 5d and 6d illustrate the presence of red-hot and yellow-hot radiations on the front and rear surfaces when a through-hole becomes evident in the CFRP specimen at 625 s.

As shown in Figs. 5b and c and 6b and c, the temperature distribution appeared lower at 312 s compared to earlier stages 156 s. This can be attributed to the thermal dynamics of the material during the laser exposure. At earlier stages (156 s), the laser energy is primarily absorbed by the CFRP, leading to higher local temperatures and more significant degradation. In contrast, at later stages (312 s), the CFRP may have

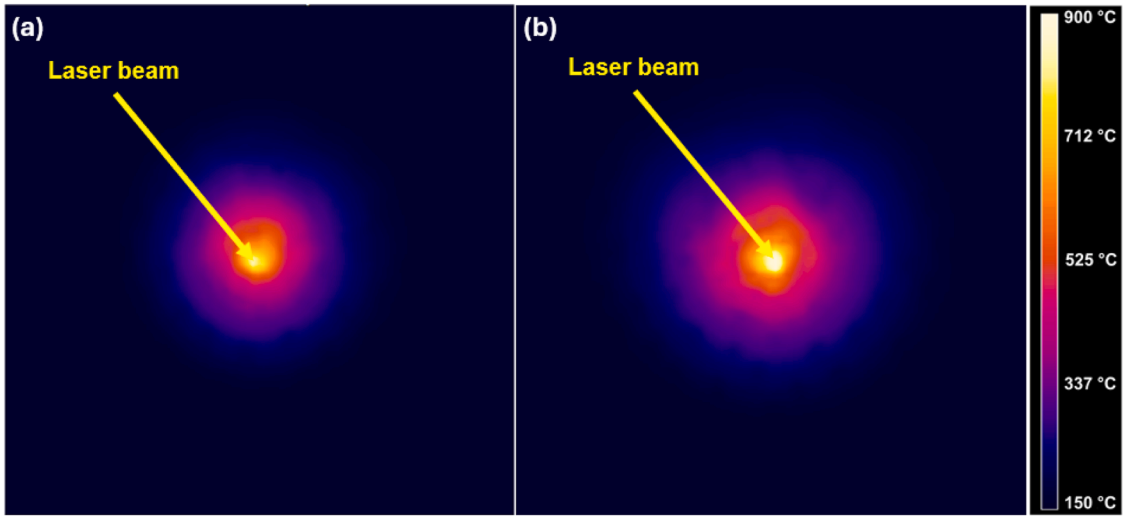

Fig. 3. Thermal imaging capturing the CFRP laminate exposed to CW laser irradiation of a) 30 W and b) 40 W; Beam diameter: 3.46 mm; Exposure time: 600 s.

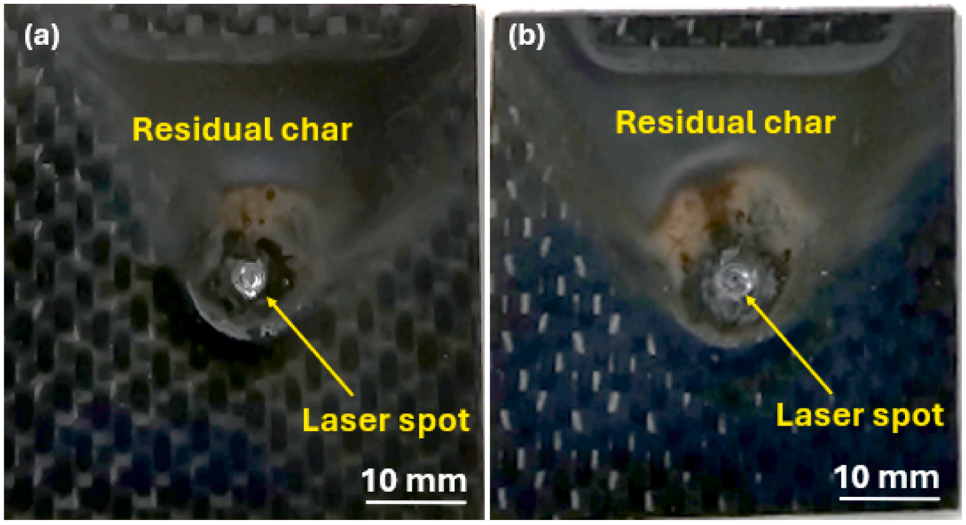

Fig. 4. Macroscopic characteristics of the laser-damaged CFRPs' front surface following 600 s of exposure with a 3.46 mm diameter beam under powers of: (a) 30 W and (b) 40 W.

already undergone some pyrolysis and matrix degradation, leading to a reduction in the CFRP ability to absorb additional heat. Additionally, heat dissipation and increased thermal conductivity through the degraded matrix could also contribute to the observed decrease in temperature at later stages.

Figs. 7 and 8 show the front and rear surface temperatures of the CFRP laminates when the specimen is exposed to a laser power of 98 W and a beam diameter of 5.70 mm. The images are captured at 60, 238, 477 and 954 s after the onset of laser irradiation. It was observed that the specimens sporadically ignited before complete perforation at 954 s, requiring a longer irradiation time of approximately 53 % for the 5.70 mm beam diameter compared to that of the 3.18 mm beam diameter. The extended exposure of the 5.70 mm laser beam was 954 s, in contrast to the 625 s penetration time for the 3.18 mm laser beam diameter. However, the thermal imaging comparisons reveal that the high-temperature area extends further under the 3.18 mm beam diameter. This can be explained by the concentrated energy delivery associated with the smaller beam diameter. The 3.18 mm beam focuses the laser energy onto a smaller surface area, resulting in a higher power density and more intense localised heating. This concentrated heating causes rapid temperature increases and a significant thermal gradient, allowing the heat to penetrate deeper into the material in a more aggressive manner. In contrast, while the 5.70 mm beam diameter does lead to prolonged heating and lateral heat transfer, the lower power density results in a more controlled and slower thermal diffusion. This distribution of energy can limit the extent of the high-temperature region, despite the larger HAZ in terms of its lateral spread.

Fig. 9 presents a comparison of the CFRP specimen temperatures measured by the thermal imaging cameras against laser irradiation time for the front (Fig. 9a) and rear surfaces (Fig. 9b). The temperatures shown in the figure represent the maximum temperature at the centre of the sample, specifically at the laser irradiation point, as recorded by the thermal imaging cameras. As depicted in Fig. 9a, the front surface temperature exceeded 2000 °C almost immediately due to the high power intensity associated with a 3.18 mm beam diameter. Since the front thermal imaging camera has a maximum measurable limit of 2000 °C, it was unable to capture the peak temperature of the front surface. Conversely, with a 5.70 mm beam diameter, the front surface temperature increased more gradually, attributed to the lower heat flux, and eventually reached 2000 °C after approximately 870 s. For the temperatures measured, particularly at the rear surface, it can be observed that the specimen subjected to a larger beam diameter, and hence lower

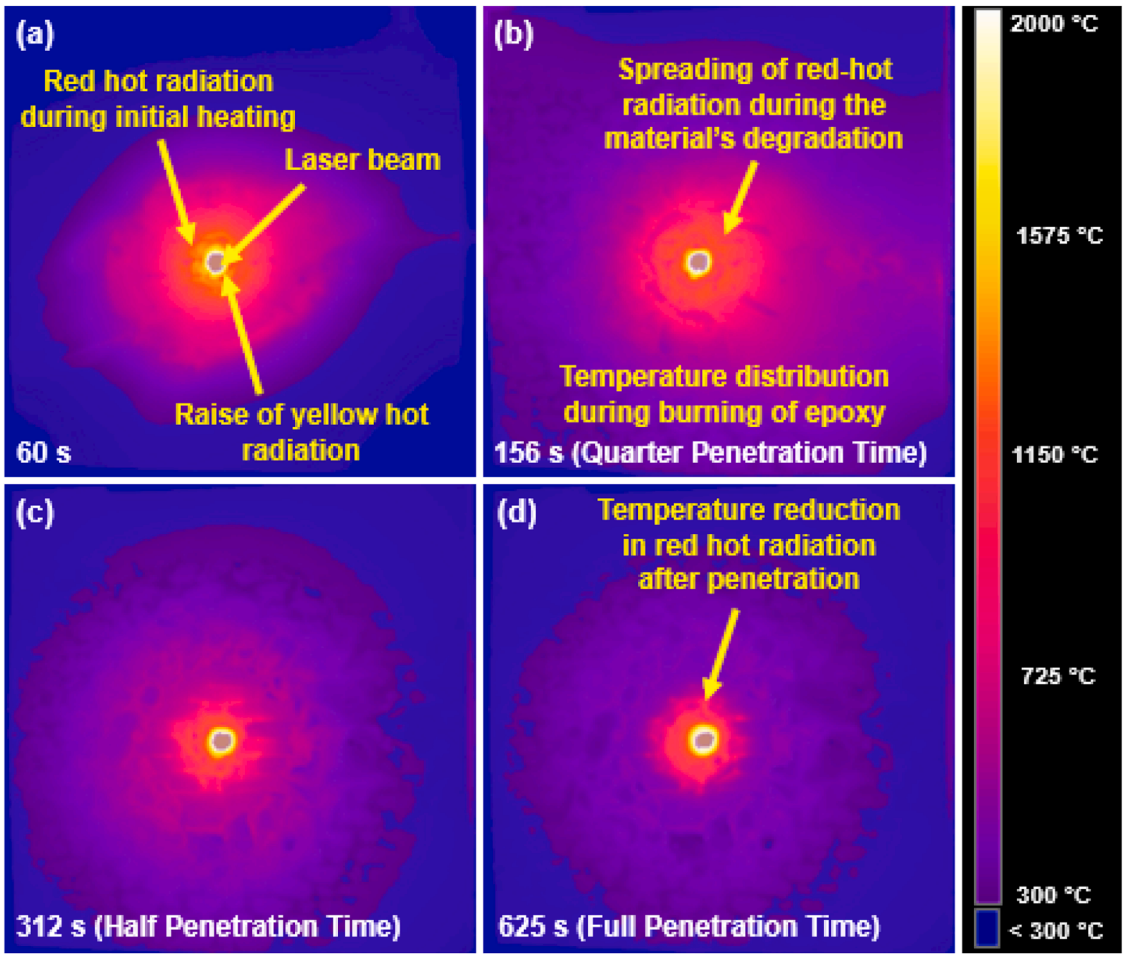

Fig. 5. Thermal imaging capturing the temperature distribution on the front surface of the CFRP laminate exposed to CW laser irradiation. Laser power: 98 W; Beam diameter: 3.18 mm; Perforation time: 625 s.

heat flux, has its temperatures lag behind the specimen with the smaller beam diameter, resulting in a significantly increased irradiation time for perforation to occur. In Fig. 9b, the first peaks in temperature occur at around their quarter penetration time due to the matrix degradation. After the matrix degradation, the maximum temperature reduces until peaking again when perforation occurs as the carbon fibre burns up.

3.4. Macro-morphology of the 98 W laser power irradiated CFRP laminate specimens

The macro-morphologies of the front and rear surfaces of the laser irradiated CFRP laminates are presented in Fig. 10. The damage appears nearly circular due to the carbon fibre weave, which promotes symmetric heat transfer. The HAZ increased with exposure time as carbon fibres absorb energy, leading to epoxy crosslinking or decomposition [29,30]. Flames observed during irradiation are attributed to epoxy combustion, often resulting in charring (Fig. 10). For the 3.18 mm beam (Fig. 10a), minor charring is evident, whereas the 5.70 mm beam (Fig. 10c) exhibits substantial charring. The larger beam diameter extends epoxy combustion, intensifying char formation and fibre delamination. Although the charring boundary is less distinct in Fig. 10c and 10d, the more extensive HAZ and charring are evident. The prolonged exposure enhances heat transfer, accelerating resin degradation and char formation. These macroscopic observations are supported by SEM analysis (Section 3.6.1), which reveals increased residual char and delamination in specimens irradiated with the 5.70 mm beam.

The less distinct boundary of charring in Fig. 10a could be due to the gradual transition between charred and unaffected areas, as opposed to a sharply defined edge. Additionally, the larger beam diameter results in a broader area of thermal impact, which can cause a more diffuse and less clearly delineated charring zone compared to smaller beam diameters. Thus, while the clear boundary of charring may be difficult to visualise, the microscopic evidence from SEM analysis supports the conclusion that the 5.70 mm beam diameter induces a more extensive HAZ, and greater charring compared to the smaller beam diameter.

3.5. Effect of beam diameter on damage extent for the 98 W laser power irradiated CFRP laminates specimens

The mass loss in CFRP laminates under laser irradiation is influenced by the heat flux that determines the spatial distribution of laser energy. The two beam diameters used of 3.18 mm and 5.70 mm, resulted in varying laser intensities of nominally 24.7 W/mm^2 and 7.68 W/mm^2, respectively. As shown in Fig. 11, for the 3.18 mm beam diameter (higher laser intensity), the mass loss increases from 30 % (±1 %) after 156 s of exposure to 40 % (±1 %) after 625 s. The higher laser intensity results in more concentrated energy on the CFRP surface, leading to accelerated thermal degradation, including resin decomposition and carbon fiber sublimation. In contrast, the 5.70 mm beam diameter (lower laser intensity) produces a slower rate of mass loss. After 238 s, the mass loss is 14 % (±3 %), and after 954 s, it reaches 31 % (±8 %). The lower laser intensity results in less aggressive degradation; however, prolonged exposure allows a thicker char layer to form on the surface, acting as a thermal barrier. This char reduces further material loss by slowing heat penetration, thereby decreasing the recorded mass loss despite more extensive internal damage.

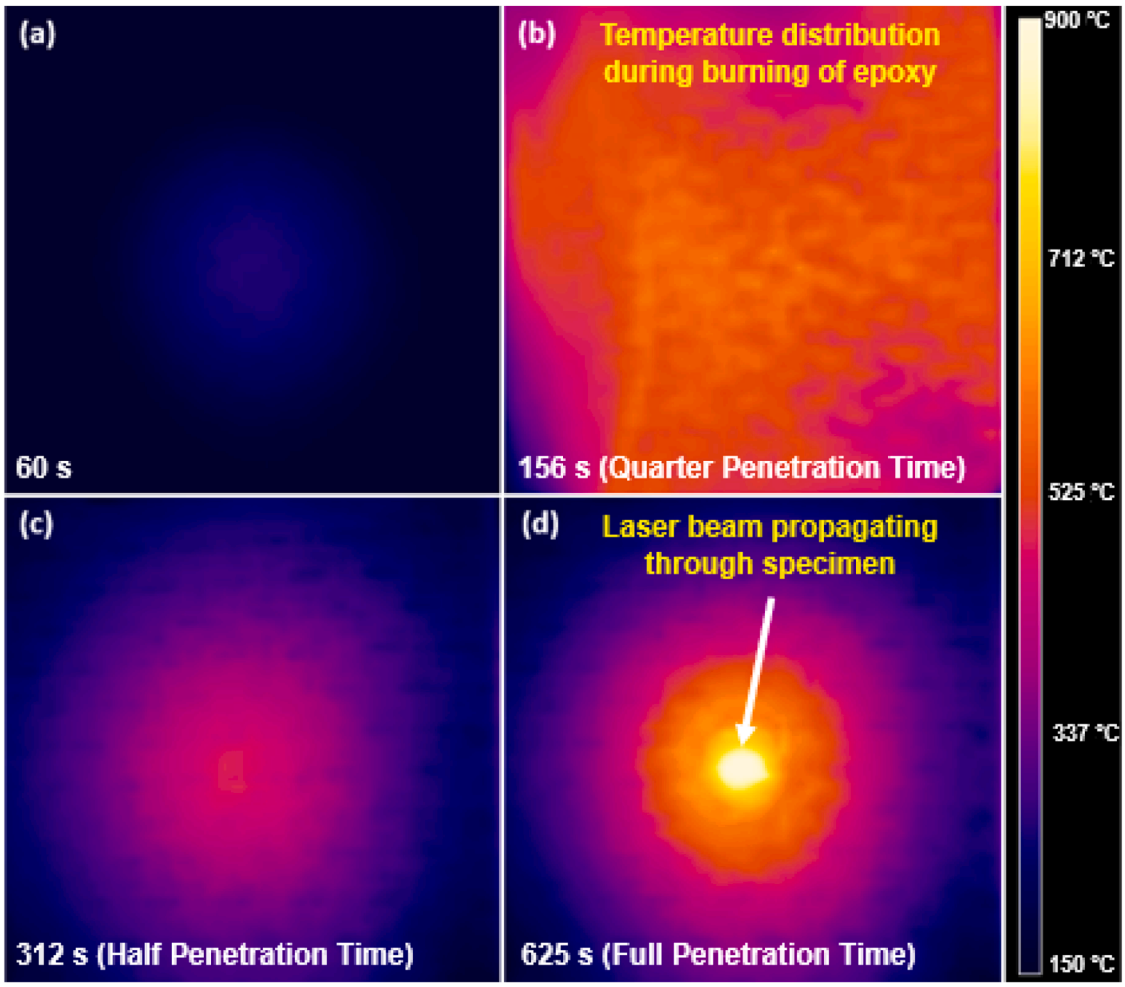

Fig. 6. Thermal imaging capturing the temperature distribution on the rear surface of the CFRP laminate exposed to CW laser irradiation. Laser power: 98 W; Beam diameter: 3.18 mm; Perforation time: 625 s.

3.6. Microstructural analysis of the 98 W laser power irradiated CFRP laminate specimens

3.6.1. SEM analysis

Fig. 12 presents SEM images of the front surface morphology of CFRP specimens subjected to laser irradiation at different exposure times using a 3.18 mm beam diameter (Fig. 12a–c) and a 5.70 mm beam diameter (Fig. 12d–f). Within the irradiated region, both the carbon fibres and epoxy matrix undergo burning or chipping, resulting in a cone-shaped perforation. The hole diameter, defined as the region where carbon fibres are fully removed, is initially smaller than the beam diameter but increases with prolonged exposure due to progressive material loss. In the surrounding HAZ, the epoxy matrix is absent on the front surface, while the carbon fibres remain largely intact. Residual char observed on both the front and rear surfaces (Fig. 10) suggests significant thermal degradation and epoxy ablation, indicating that laser-induced damage extends beyond the top layer into the composite structure. A detailed examination of the hole edge reveals broken carbon fibres coated with residual matrix particles, indicating initial chipping and intense smoke formation due to thermally induced stresses [32]. With increased exposure time, fewer chipping fragments are observed, while oxidation-driven degradation of the matrix and fibres becomes more dominant, reducing smoke formation but enhancing overall material loss.

Fig. 13 shows SEM images of CFRP specimens at different damage regions for the 3.18 mm (Fig. 13a–c) and 5.70 mm (Fig. 13d–f) beam diameters. In the hole region (Fig. 13a, 13d), carbon fibres exhibited pointed ends and minimal matrix residue, indicating exposure to high temperatures. Wolfrum et al. [32] noted a decrease in carbon fibre diameter by ~1 μm near the ends and surface roughening, which were typical characteristics of oxidation-induced degradation. TGA results (Fig. 2) showed that carbon fibre degradation began above 660 °C in oxygen, while matrix degradation started at ~300 °C within minutes. However, laser irradiation generated significantly higher temperatures in a short time. In Fig. 13b, the 3.18 mm beam created subtle residual char, while Fig. 13e showed more substantial char for the 5.70 mm beam due to prolonged exposure. Extended exposure intensified char formation and contributed to greater delamination within the laminate. The damage areas near the edge of the 3.18 mm (Fig. 13c) and 5.70 mm (Fig. 13f) beam diameter laser-irradiated CFRP specimens indicated that the laser primarily ablated the surface epoxy layer, leaving the exposed fibres intact. The deeper epoxy layers remained partially unaffected due to temperature variations across the laminate thickness. Residual char exhibited a porous structure, suggesting a higher degree of epoxy resin decomposition, while the carbon fibres appeared undamaged, implying that the temperature during irradiation did not exceed the carbon fibre sublimation threshold (Figs. 5–9). Additionally, surface cracks were observed in the edge regions, likely due to lower surface temperatures compared to the adjacent hole and near-hole regions.

The SEM analysis provided detailed insights into the surface characteristics of laser-damaged CFRP, specifically in the hole, near-hole, and near-edge regions of the specimens. The results indicate that

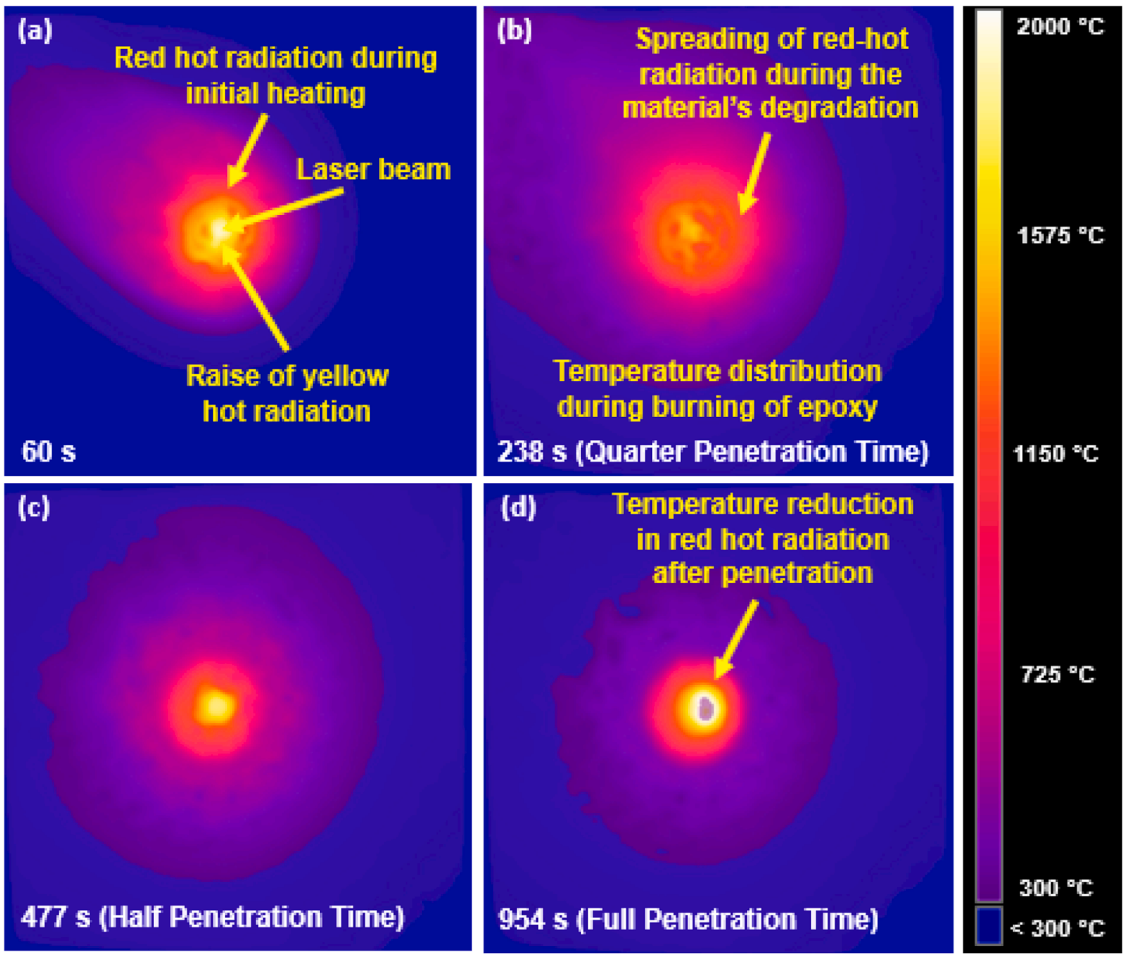

Fig. 7. Thermal imaging capturing the temperature distribution on the front surface of the CFRP laminate exposed to CW laser irradiation. Laser power: 98 W; Beam diameter: 5.70 mm; Perforation time: 954 s.

CFRP samples exposed to the 5.70 mm beam diameter exhibited greater residual char formation and epoxy ablation compared to those subjected to the 3.18 mm beam diameter. This increased thermal degradation is attributed to the longer exposure time associated with the larger beam. Additionally, the SEM images revealed fibre damage near the hole region, along with residual char and surface cracks, highlighting surface-level degradation mechanisms. To complement these findings, internal damage mechanisms such as delamination and intralaminar cracks were further examined using micro-CT imaging in Section 3.6.3. This advanced characterisation provided a more comprehensive assessment of the internal structural integrity of the CFRP specimens following laser irradiation.

3.6.2. *Ultrasonic analysis*

Ultrasonic C-scans were used to assess the lateral extent of internal damage in CFRP specimens after complete laser penetration. The 2-D C-scan colour maps (Fig. 14) provided details on acoustic reflection and transmission, revealing structural integrity and damage mechanisms following laser irradiation with 3.18 mm and 5.70 mm beam diameters. Fig. 14a and 14b show the reflection and transmission images of the pristine CFRP, with slight variations in the reflection strength due to changes in fibre volume fraction or large resin pockets, typical for fibre-reinforced composites. In contrast, the reflection images of laser-damaged CFRP (Fig. 14c and 14e) showed high acoustic reflection from internal air defects, particularly within circular regions corresponding to laser penetration zones. These air gaps, resulting from thermal degradation of the matrix resin and carbon fibres, indicate voids and delamination, compromising the structural integrity of the CFRP.

Transmission scans (Fig. 14d and 14f) revealed areas of high transmission in regions of improved structural soundness, except at the central hole, where complete penetration led to zero reflection and high transmission due to the absence of structural material and matrix resin. Throughout the specimens, transmission scans primarily showed low transmission (blue), indicating extensive resin evaporation. However, near the laser-induced hole, variations in transmission were observed, suggesting that residual char and re-fused carbon fibres replaced initial air voids, altering acoustic properties and enabling more ultrasound transmission. These results highlight the complex nature of CFRP degradation under laser irradiation, with ultrasonic C-scan analysis visualising internal defects and characterising their extent. Future research could refine these techniques to enhance sensitivity and spatial resolution for better assessments of material conditions and improvements in composite design for enhanced durability under thermal conditions.

3.6.3. *Micro-CT analysis*

Fig. 15 presents micro-CT scans of the front surface and cross-sectional views of both pristine and laser-damaged CFRP samples subjected to full penetration by laser irradiation at 98 W power, using 3.18 mm and 5.70 mm beam diameters. Figs. 15a and 15d show the front surface and cross-sectional images of the pristine specimen, revealing porosity and internal defects. Figs. 15b and 15e display the front surface and cross-sectional views of CFRP damaged by the 3.18 mm beam diameter, while Figs. 15c and 15f show the corresponding views for CFRP damaged by the 5.70 mm beam diameter. Voids within the material may act as stress concentrators during laser irradiation. With the

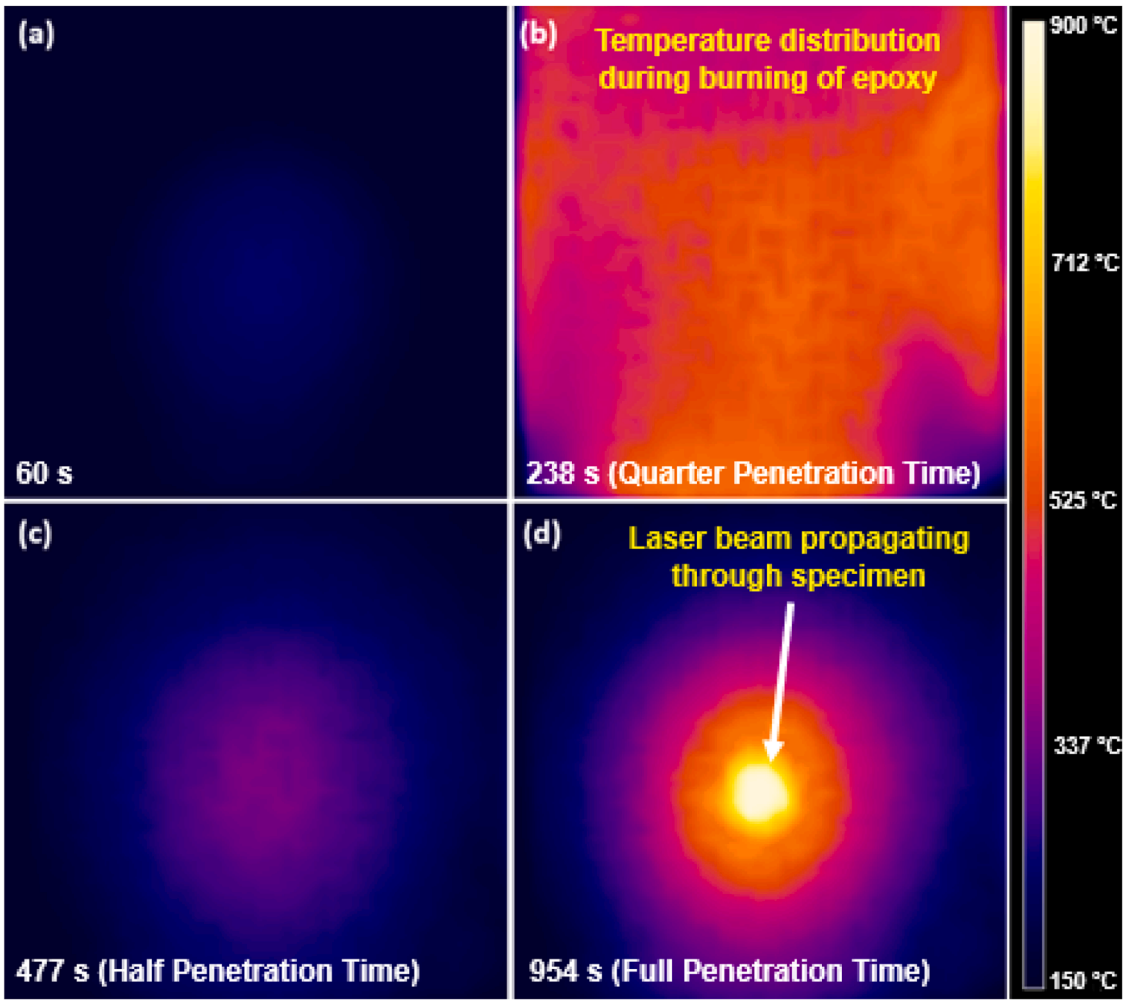

Fig. 8. Thermal imaging capturing the temperature distribution on the rear surface of the CFRP laminate exposed to CW laser irradiation. Laser power: 98 W; Beam diameter: 5.70 mm; Perforation time: 954 s.

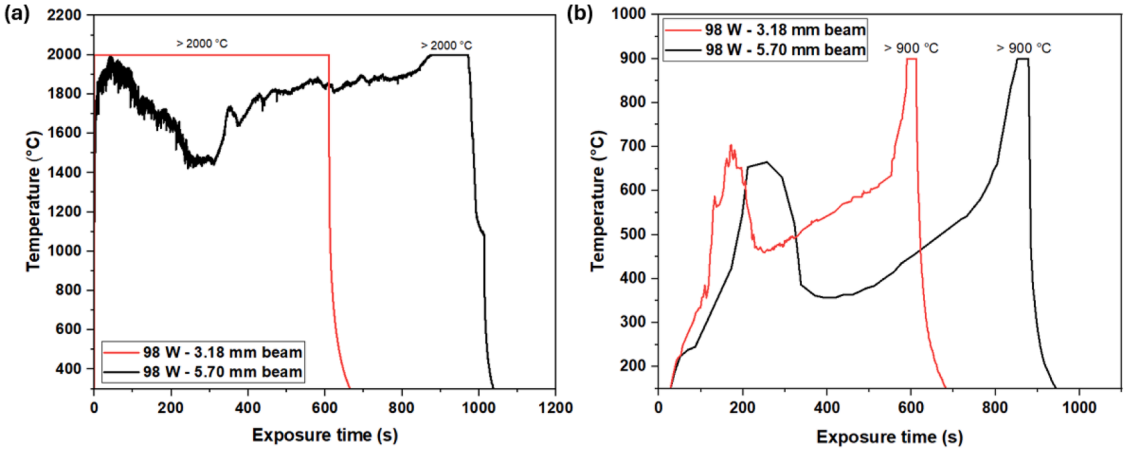

Fig. 9. The variation of the CFRP laminates' temperature to the beam diameter and exposure time under 98 W CW laser irradiation: (a) front surface, and (b) rear surface.

3.18 mm beam diameter, concentrated energy induces rapid localised heating, leading to the immediate vaporisation of the resin within the pores. This results in increased mass loss, expulsion of volatile compounds, and accelerated degradation of the polymer matrix, contributing to the formation of larger voids, cracks, and micro-delamination. This process significantly increases the material's porosity, thereby compromising its mechanical properties. In contrast, the 5.70 mm beam diameter distributes energy over a broader area, producing a slower, more gradual heating effect. Although mass loss is initially lower, prolonged exposure allows for sustained thermal degradation, leading to

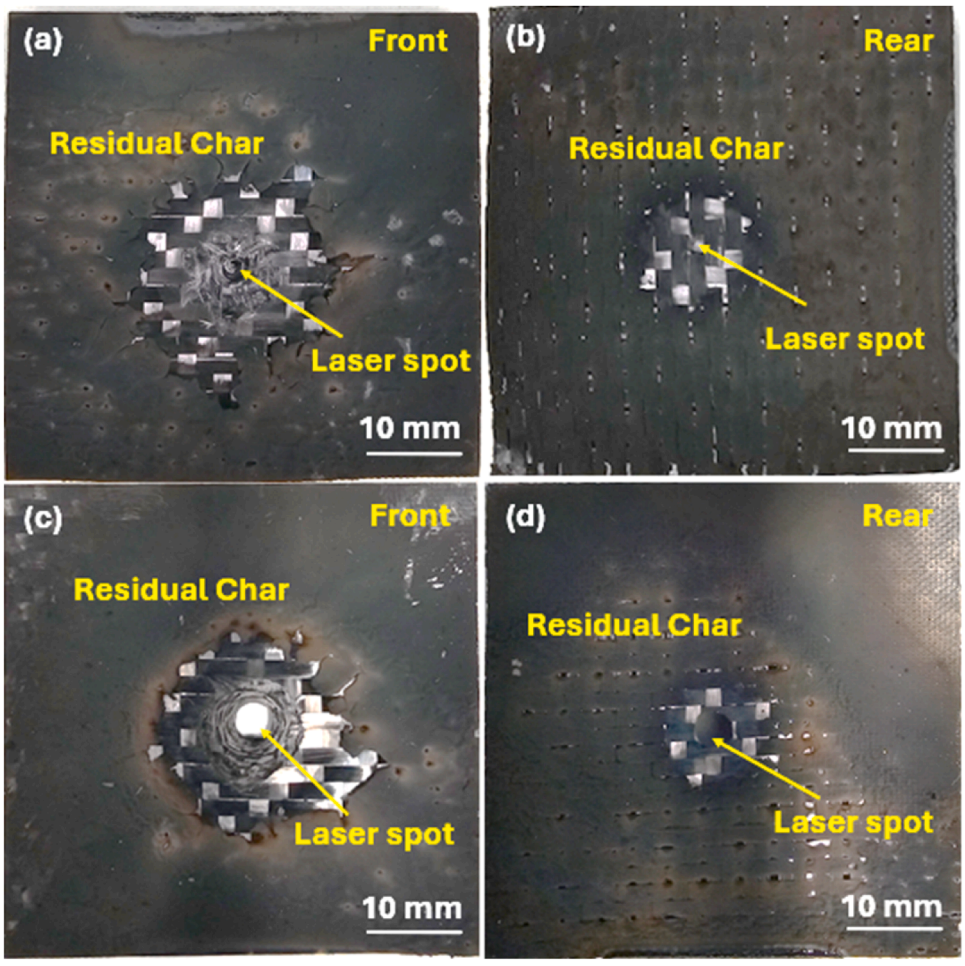

Fig. 10. Macroscopic characteristics of the laser damaged CFRP laminates' front and back surfaces following complete perforation under a laser power of 98 W different beam diameters: (a, b) 3.18 mm and (c, d) 5.70 mm.

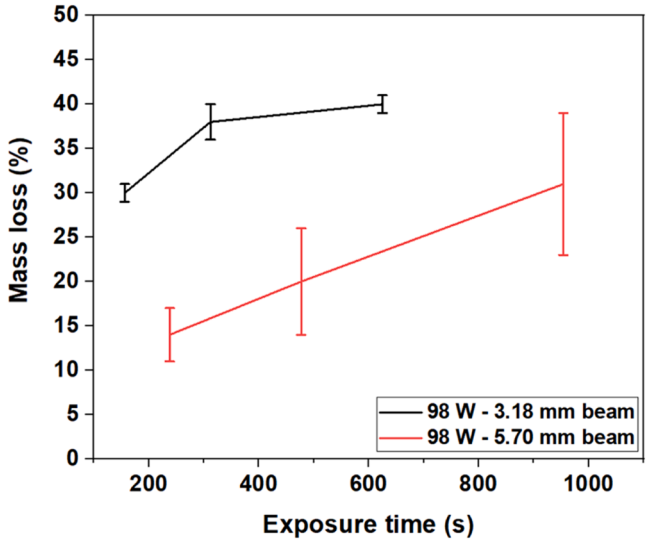

Fig. 11. Variation in mass loss of CFRP laminates under exposure to a 98 W laser power with beam diameters of 3.18 mm and 5.70 mm across different exposure times.

char formation that may temporarily fill some of the pores. However, this does not provide sufficient structural integrity over time. While slower heating reduces immediate resin vaporisation, it permits sustained thermal stress, resulting in more severe internal damage, as observed in Figs. 15b and 15c.

The front surface scan reveals areas of matrix decomposition (depicted in black), while the white regions correspond to the epoxy matrix and carbon fibres. On the other hand, the cross-sectional images highlight layer separation and interlaminar cracks (shown in black), with the white regions representing the matrix and fibres. The front surfaces of both laser-damaged specimens show that the epoxy matrix was decomposed significantly throughout the specimen. During laser irradiation, CFRPs experience physical and chemical changes involving heat conduction, convection, and radiation. These transformations entail the pyrolysis of the epoxy matrix, oxidation, and sublimation of carbon fibres, thermomechanical erosion, and the occurrence of delamination induced by thermal stresses (interlayer cracking) [33,38]. From Fig. 2, it was observed that the epoxy degradation occurred between 300 °C and 500 °C. The matrix degradation involves the absorption of heat, the release of gas, and the formation of pyrolytic carbon. The breakdown of the polymer matrix results in the loss of its structural integrity, which is referred to as matrix decomposition. During this process, there is a reduction in the polymer phase (matrix) and an increase in the residual char (Fig. 13) leading to a rise in gas pressure. When this pressure reaches a specific threshold, it is released into the surrounding atmosphere [20].

The cross-sectional images reveal a hole created by the laser beam, tapering conically from the front to the rear surface (Fig. 15e and 15f). The ablation centre and surrounding HAZ follow distinct temperature gradients, with the highest temperatures at the centre, leading to a cone-

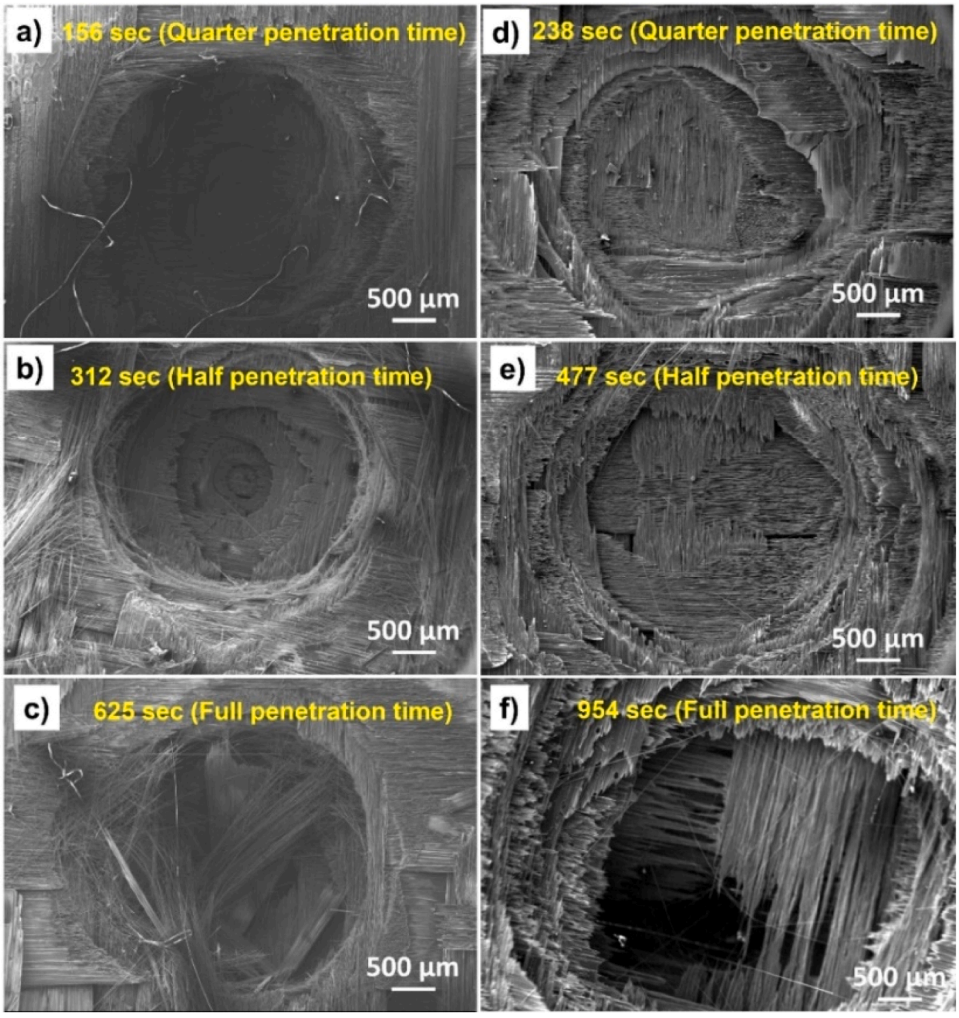

Fig. 12. SEM images of CFRP specimens irradiated at 98 W for different periods with 3.18 mm (a, b, c) and 5.70 mm (d, e, f) beam diameters within the laser spot region.

shaped hole as energy from the Gaussian laser beam extends into the laminate. The hole diameter on the irradiated surfaces is approximately 10 mm, increasing with longer exposure times that allow for carbon fibre decomposition. Despite lower mass loss rates with the 5.70 mm beam diameter, the larger beam leads to greater material loss due to more extensive HAZ and prolonged thermal damage, which becomes apparent in morphological analyses rather than mass loss measurements. Prolonged exposure with the larger beam diameter facilitates char formation and extended burning of the epoxy matrix, contributing to further material loss. While the larger beam results in slower evaporation, sustained thermal stress and lateral heat conduction cause greater damage [20]. The surrounding plies experience layer separation due to resin decomposition, leading to outward expansion, particularly on the rear surface. This is more pronounced with the 5.70 mm beam, where higher temperatures have a greater effect. Longer exposure times result in a wider Gaussian-shaped area of thermal damage and delamination, as heat conduction plays a critical role in the damage mechanism. The larger beam diameter thus shows more pronounced expansion due to delamination. The process begins with matrix degradation, leading to delamination, followed by carbon fibre removal. Near the edge, partial pyrolysis and melting of the epoxy resin form fine cracks in the interlaminar zone (Fig. 15e and 15f). Liu et al. [34], observed interlaminar failure influenced by thermal stresses, with cracks forming near the rear surface where no matrix decomposition occurs. The thermal decomposition of the epoxy and carbon fibres generates gases, increasing internal pressure. When this pressure exceeds a critical threshold, it leads to micro-cracking and delamination, as localised heating and expansion create internal stresses that exceed the cohesive strength of the CFRP [39].

The results of this study are directly relevant to industrial applications involving laser-material interactions, such as laser cleaning and machining. The findings demonstrate that a smaller beam diameter (3.18 mm) leads to intense localised heating, causing rapid resin vaporisation and fibre sublimation. This effect is beneficial in laser machining for precise material removal but may also weaken the structural integrity of CFRP. In contrast, a larger beam diameter (5.70 mm) distributes heat over a wider area, resulting in prolonged exposure times and extensive HAZ. While this is advantageous for laser cleaning applications, excessive thermal exposure can lead to delamination and internal cracking, reducing the mechanical performance of the material. The mechanical performance of the material is also further reduced by the laser-irradiated through hole and areas of burnt-off epoxy within in the heat affected region. When the epoxy is removed from the sample, there is no matrix to hold the fibres in place that distribute applied stresses to the material. This damage reduces the tensile and compressive strength of the composite [40]. These results highlight the need to optimise laser parameters to balance efficiency and material integrity. Additionally, mitigation strategies such as high-temperature-resistant coatings, nanocomposite-reinforced resins, and modified CFRP architectures could improve heat dissipation and minimise damage,

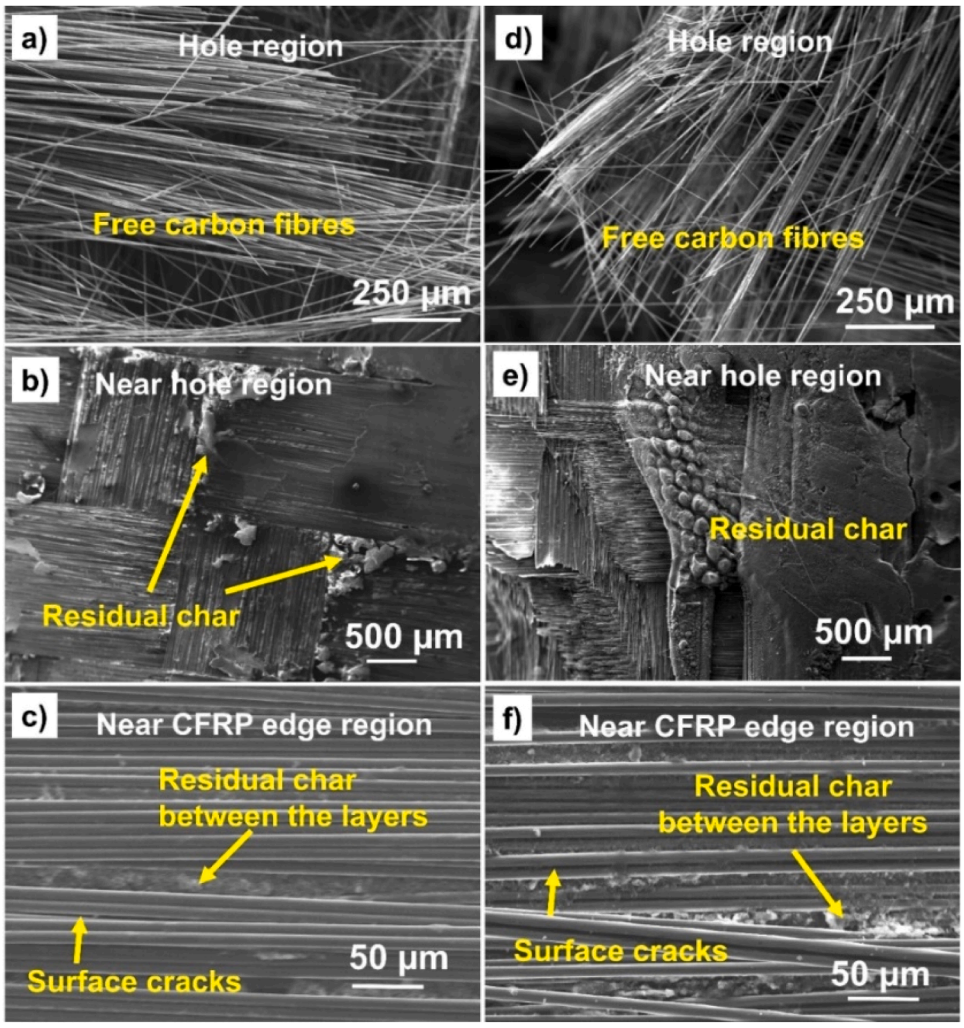

Fig. 13. SEM images of CFRP specimens showing different damage regions for 3.18 mm (a, b, c) and 5.70 mm (d, e, f) beam diameters of 98 W laser irradiation.

enhancing the durability of CFRP in laser-intensive applications.

4. Conclusions

This study investigated the impact of laser power density affected by beam diameter on the thermal response and degradation mechanisms of CFRP laminates using EA9396 epoxy as the matrix. Key findings of the CFRP specimens subjected to the 98 W laser power are listed below.

- Initial tests using 30 and 40 W lasers (3.46 mm beam diameter) revealed a clear trend between increased power and material degradation. Mass loss increased from 1.48 % to 2.71 % over 600 s, attributed to higher laser flux (6.37 to 8.45 W/mm^2), leading to more pronounced matrix degradation and partial fibre damage.
- In the 98 W laser test, the specimen exhibited more severe damage, including internal delamination and through-thickness failure, consistent with the higher energy input and intensified beam focus.
- The 3.18 mm beam diameter produced a higher power density (24.7 W/mm^2), resulting in localised heating, fibre sublimation, and increased material degradation. In contrast, the 5.70 mm beam diameter had a lower power density (7.68 W/mm^2), leading to more distributed heating and reduced fibre sublimation, though prolonged exposure still caused significant thermal damage.
- Increasing the laser beam diameter from 3.18 mm to 5.70 mm resulted in approximately 53 % longer exposure times. While the primary factor driving the observed thermal damage was the laser power density, other factors such as laser reflection and surface interactions could cause slight variations in the observed damage between the smaller and larger beam diameters. However, the laser power density remained the dominant factor determining the extent of thermal degradation, as the high emissivity of the CFRP through its black colour enhances absorption and thus influences the overall energy absorption, reinforcing the significance of power density in driving the observed damage patterns.
- The variations in beam diameter directly affected the power density, which in turn influenced the thermal degradation, as higher power density (smaller beam diameter) accelerated resin decomposition and carbon fibre sublimation.
- The increase in laser power density was correlated with more rapid and severe degradation, resulting in larger hole diameters (approximately 10 mm), sharper perforations, and faster material removal, demonstrating the influence of laser intensity.
- Prolonged exposure to higher laser power densities (smaller beam diameter) caused increased mass loss in the CFRP laminates, ranging from 14 % to 40 %, with more pronounced degradation under higher power density conditions. The higher power densities resulted in more localised heating, causing faster resin vaporisation, fibre degradation, and increased material loss. This intensified thermal degradation, leading to more severe internal damage, such as void formation, delamination, and structural weakening.
- Surface and subsurface damage in CFRP under laser irradiation varied with laser power density. Higher power densities caused

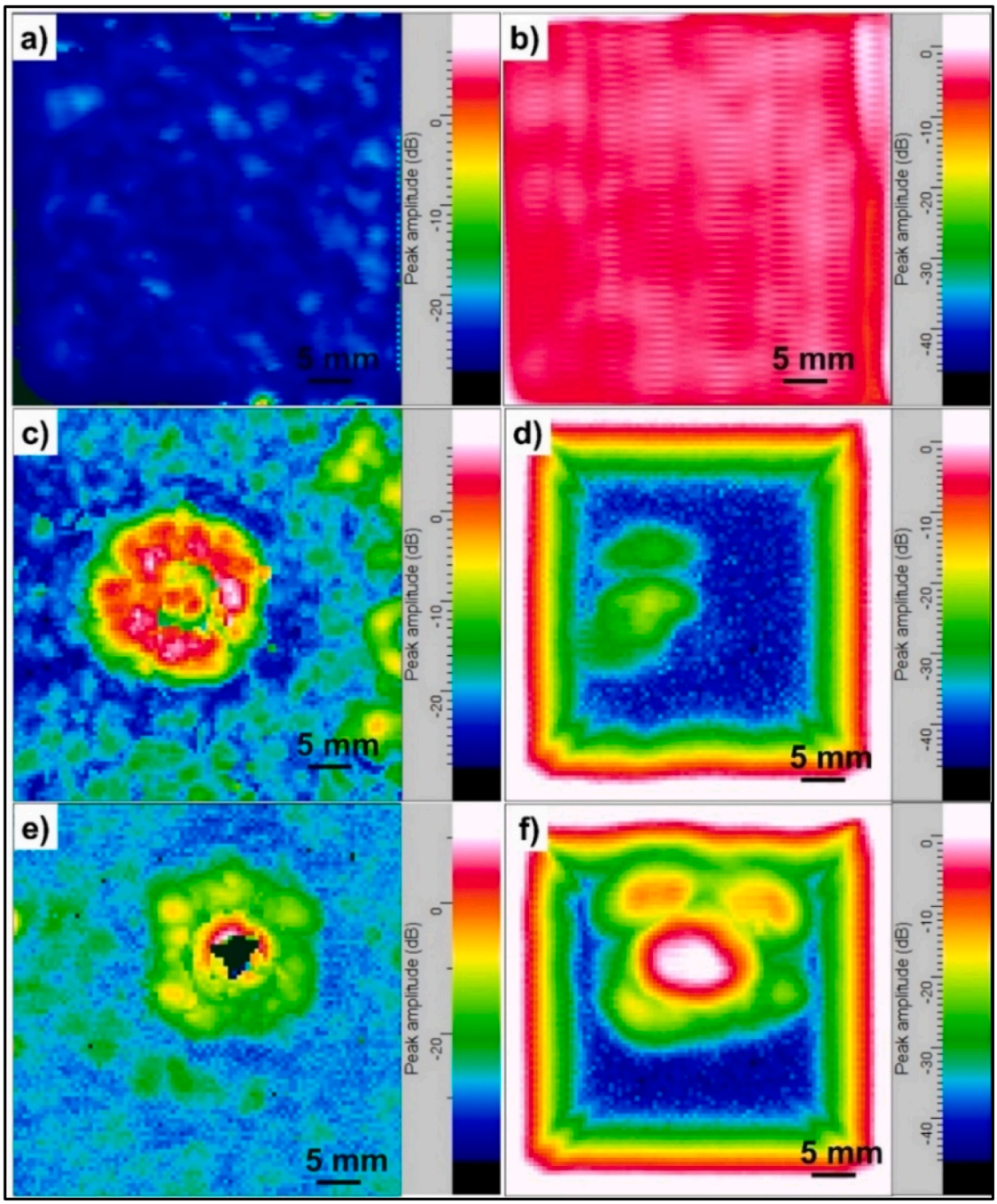

Fig. 14. Ultrasonic reflection (a, c, e) and through-thickness transmission (b, d, f) C-scans of CFRP specimens irradiated with a 98 W laser. (a, e) shows the pristine CFRP. (c, d) shows the CFRP damaged by the 3.18 mm beam diameter laser. (e, f) shows the CFRP damaged by the 5.70 mm beam diameter laser.

rapid, localised damage, including resin vaporisation, interlaminar cracking, and fibre degradation due to intense heating. Lower power densities resulted in slower heating, leading to delamination, char formation, and prolonged structural weakening.

These findings demonstrate the complex relationship between power density and degradation, offering valuable insights for optimising laser processing in applications like surface modification and machining, where controlled damage is crucial for maintaining material integrity. It should be noted that in this research, laser powers of 30 W, 40 W and 98 W were studied to understand the effect of laser irradiation over extended exposure times. Comparing the beam diameters fixed at 98 W aimed to compare the damage mechanisms that occur via comprehensive microscale testing and analysis via advanced characterisation methods. Testing with a broad range of relatively higher laser powers up to 365 W as well as studies involving damage mitigation strategies via the use of additives will be conducted and reported in the future.

CRediT authorship contribution statement

Patrick K. Kamlade: Writing – review & editing, Writing – original draft, Validation, Methodology, Investigation, Formal analysis, Conceptualization. **Jojibabu Panta:** Writing – review & editing, Writing – original draft, Validation, Methodology, Investigation, Formal analysis, Conceptualization. **Max Mammone:** Investigation. **Richard**

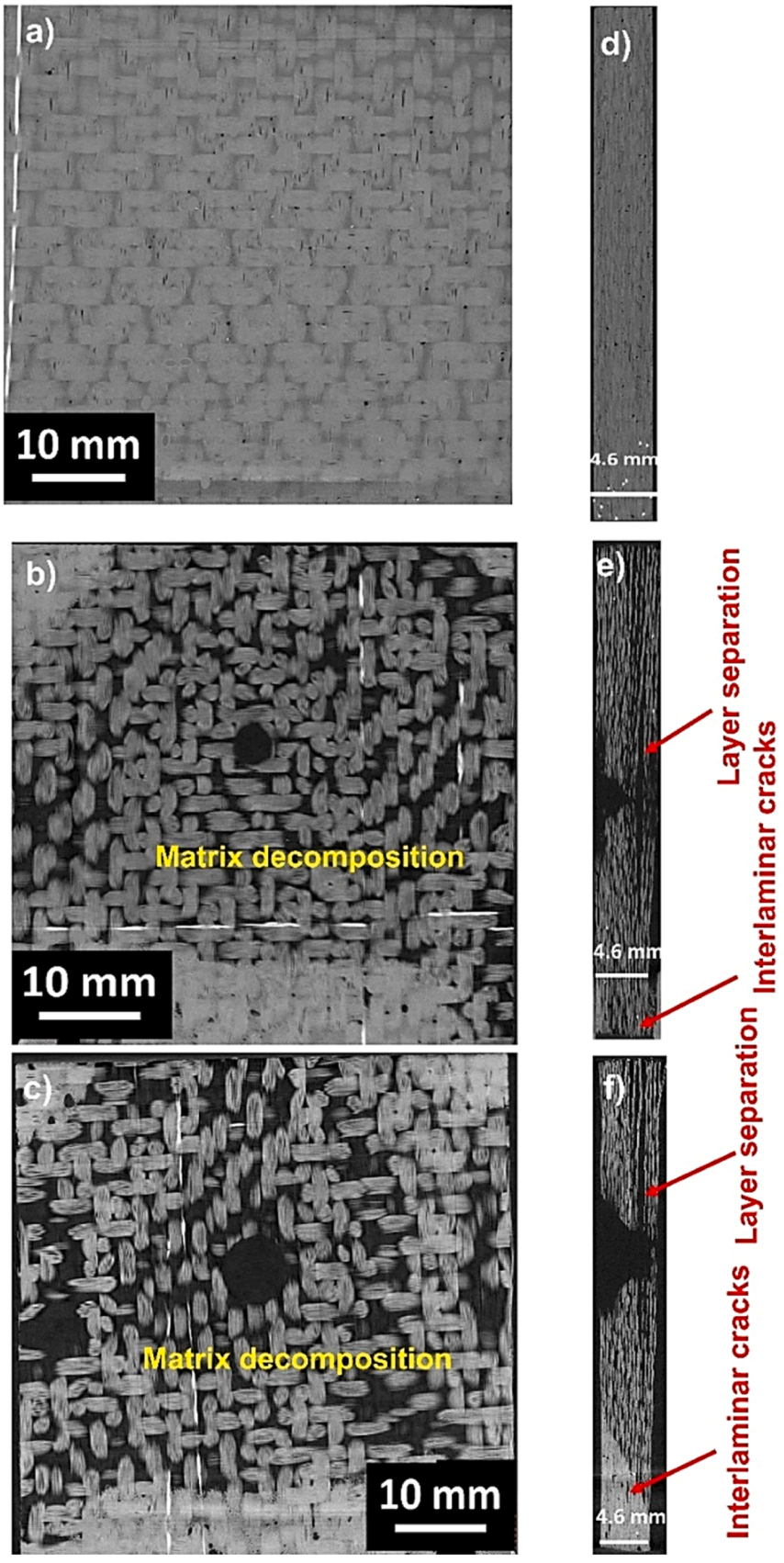

Fig. 15. Micro-CT of CFRP specimens irradiated with a 98 W laser. The front surface and cross-sectional view are respectively shown for: (a, d) the pristine CFRP; (b, e) the CFRP damaged by a 3.18 mm diameter beam; and (c, f) the CFRP damaged by a 5.70 mm diameter beam.

(Chunhui) Yang: Writing – review & editing, Supervision, Funding acquisition. **Richard P. Mildren:** Writing – review & editing, Supervision, Funding acquisition. **John Wang:** Writing – review & editing, Supervision, Funding acquisition. **Matthew Ibrahim:** Writing – review & editing, Investigation, Formal analysis. **Rodney Thomson:** Writing – review & editing, Supervision, Funding acquisition. **Y.X. Zhang:** Writing – review & editing, Supervision, Project administration, Funding acquisition, Conceptualization.

Declaration of competing interest

The authors declare that they have no known competing financial interests or personal relationships that could have appeared to influence the work reported in this paper.

Acknowledgements

The authors would like to thank the Australian Defence Next Generation Technology Fund (NGTF) for supporting this project financially. The PhD scholarship from the Defence Innovation Network (DIN) and Western Sydney University awarded to Patrick Kamlade is acknowledged. The authors would like to acknowledge the Advanced Materials Characterisation Facility (AMCF) for support with the TGA and SEM studies. Additional SEM analysis was conducted at the Defence Science and Technology Group (DSTG). The authors also thank Mojtaba Moshkani from Macquarie University for providing training on the laser equipment, Adam Sharpe for assisting with the laser testing, and Greg Surtees from DSTG for his support with the micro-CT studies. Feedback and input from other project team members Emily Groves (DSTG), Lance McGarva (Airbus Australia Pacific), Juan Pablo Escobedo-Diaz (UNSW) and Ryan Campbell (ACS Australia) are also acknowledged.

Supplementary materials

Supplementary material associated with this article can be found, in the online version, at doi:10.1016/j.jcomc.2025.100605.

Data availability

Data will be made available on request.

References

[1] X. Kong, Y. Wang, X. Liu, Z. Dang, M. Wang, Research on the removal mechanism and surface damage of laser assisted cutting of CFRP materials, J. Manuf. Process. 124 (2024) 196–211.
[2] J. Gu, X. Su, Y. Jin, D. Zhang, W. Li, J. Xu, B. Guo, Research progress and prospects of laser cleaning for CFRP: a review, Compos. A: Appl. Sci. Manuf. 185 (2024) 108349.
[3] G.Kumar Rampal, S.M. Rangappa, S. Siengchin, S. Zafar, A review of recent advancements in drilling of fiber-reinforced polymer composites, Compos. C: Open Access 9 (2022) 100312.
[4] G.K. Ze, A. Pramanik, A.K. Basak, C. Prakash, S. Shankar, N. Radhika, Challenges associated with drilling of carbon fiber reinforced polymer (CFRP) composites-A review, Compos. C: Open Access 11 (2023) 100356.
[5] M. Ramachandrarao, S.H. Khan, K. Abdullah, Carbon nanotubes and nanofibers – reinforcement to carbon fiber composites - synthesis, characterizations and applications: a review, Compos. C: Open Access 16 (2025) 100551.
[6] M. Li, X. Jia, L. Gao, Z. Ma, C. Zheng, Investigation on the laser irradiation stability of epoxy resin-based composites with different Fiber structures, Polym. Degrad. Stab (2025) 111250.
[7] X. Jia, J. Luo, C. Guo, Z. Li, Z. Ma, Y. Xiang, Z. Yi, K. Li, C. Wang, X. Li, K. Han, J. a. Duan, High-energy continuous wave laser ablation of alumina ceramic, J. Mater. Res. Technol. 27 (2023) 5389–5403.
[8] Y. Zhen, Z. Ma, L. Gao, D. Wang, C. Wei, Y. Lv, Z. Zhang, H. Liu, Y. Wang, W. Xu, Ablation behavior and microwave absorption performance of metamaterials irradiated by high-energy continuous-wave laser, Mater. Des. 225 (2023) 111502.
[9] C. Ma, Z. Ma, L. Gao, Y. Liu, J. Wang, M. Song, F. Wang, H. Ishida, Laser ablation behavior of nano-copper particle-filled phenolic matrix nanocomposite coatings, Compos. B: Eng. 155 (2018) 62–68.
[10] F.O. Olsen, L. Alting, Pulsed laser Materials processing, ND-YAG versus CO2 lasers, CIRP Ann. 44 (1995) 141–145.
[11] N. Rajaram, J. Sheikh-Ahmad, S.H. Cheraghi, CO2 laser cut quality of 4130 steel, Int. J. Mach. Tools Manuf. 43 (2003) 351–358.
[12] C. Leone, S. Genna, V. Tagliaferri, Fibre laser cutting of CFRP thin sheets by multi-passes scan technique, Opt. Lasers Eng. 53 (2014) 43–50.
[13] J. Limpert, A. Liem, H. Zellmer, A. Tünnermann, 500 W continuous-wave fibre laser with excellent beam quality, Electron. Lett. 39 (2003) 1.
[14] T.M. Pollak, W. Wing, R. Grasso, E. Chicklis, H. Jenssen, CW laser operation of Nd: YLF, IEEE J. Quantum Electron. 18 (1982) 159–163.
[15] P. Nan, Z. Shen, B. Han, X. Ni, The influences of laminated structure on the ablation characteristics of carbon fiber composites under CW laser irradiation, Opt. Laser Technol. 116 (2019) 224–231.
[16] J.R. Cook, Atmospheric propagation of high energy lasers and applications, in: AIP Conference Proceedings, American Institute of Physics, 2005, pp. 58–72.
[17] C.D. Boley, A.M. Rubenchik, Modeling of laser interactions with composite materials, Appl. Opt. 52 (2013) 3329–3337.
[18] M. Li, S. Li, X. Yang, Y. Zhang, Z. Liang, Effect of lay-up configuration and processing parameters on surface quality during fiber laser cutting of CFRP laminates, Int. J. Adv. Manuf. Technol. 100 (2019) 623–635.
[19] C. Leone, E. Mingione, S. Genna, Laser cutting of CFRP by Quasi-Continuous Wave (QCW) fibre laser: effect of process parameters and analysis of the HAZ index, Compos. B: Eng. 224 (2021) 109146.
[20] Q. Chai, Y. Luo, X. Qian, Y. Zhang, L. Zhao, Investigation on ablative process of CFRP laminates under laser irradiations, Opt. Laser Technol. 174 (2024) 110687.
[21] D. Herzog, P. Jaeschke, O. Meier, H. Haferkamp, Investigations on the thermal effect caused by laser cutting with respect to static strength of CFRP, Int. J. Mach. Tools Manuf. 48 (2008) 1464–1473.
[22] K. Kerrigan, G.E. O'Donnell, On the relationship between cutting temperature and workpiece polymer degradation during CFRP edge trimming, Procedia CIRP 55 (2016) 170–175.
[23] F. Lacroix, V. Allheily, K. Diener, A. Eichhorn, M. Gillet, G. L'Hostis, Thermomechanical behavior of aeronautic structural carbon epoxy composite submitted to a laser irradiation, Compos. Struct. 143 (2016) 220–229.
[24] S. Affan Ahmed, M. Mohsin, S.M. Zubair Ali, Survey and technological analysis of laser and its defense applications, Def. Technol. 17 (2021) 583–592.
[25] F. Fischer, S. Kreling, P. Jäschke, M. Frauenhofer, D. Kracht, K. Dilger, Laser surface pre-treatment of CFRP for adhesive bonding in consideration of the absorption behaviour, J. Adhes. 88 (2012) 350–363.
[26] A. Wolynski, T. Herrmann, P. Mucha, H. Haloui, J. L'huillier, Laser ablation of CFRP using picosecond laser pulses at different wavelengths from UV to IR, Phys. Procedia 12 (2011) 292–301.
[27] S. Sihn, J. Pitz, J.P. Vernon, Laser-induced heating, property changes, and damage modes in carbon fiber reinforced polymer matrix woven composites, Compos. Struct. 322 (2023) 117422.
[28] M. Mammone, J. Panta, R.P. Mildren, J. Wang, J. Escobedo-Diaz, L. McGarva, M. Ibrahim, A. Sharp, R. Yang, Y.X. Zhang, Advanced characterization of thermal degradation mechanisms in carbon fibre-reinforced polymer composites under continuous wave laser irradiation, Compos. A: Appl. Sci. Manuf. 192 (2025) 108817.
[29] E. Gay, L. Berthe, M. Boustie, M. Arrigoni, E. Buzaud, Effects of the shock duration on the response of CFRP composite laminates, J. Phys. D Appl. Phys. 47 (2014) 455303.
[30] F. Fischer, S. Kreling, F. Gäbler, R. Delmdahl, Using excimer lasers to clean CFRP prior to adhesive bonding, Reinf. Plast. 57 (2013) 43–46.
[31] M. Jung, T. Riesbeck, J. Schmitz, T. Baumgärtel, K. Ludewigt, A. Graf, High energy laser demonstrators for defense applications, in: XXI International Symposium on High Power Laser Systems and Applications 2016, SPIE, 2017, pp. 271–278.
[32] J. Wolfrum, S. Eibl, E. Oeltjen, J. Osterholz, M. Wickert, High-energy laser effects on carbon fiber reinforced polymer composites with a focus on perforation time, J. Compos. Mater. 55 (2021) 2249–2262.
[33] Y. Zhang, J. Pan, S. Zhou, Q. Yin, J. Zhang, W. Xie, F. Tan, W. Zhang, Experimental investigation on ablation behaviors of CFRP laminates in an atmospheric environment irradiated by continuous wave laser, Polym. (Basel) 14 (2022) 5082.
[34] Y.-C. Liu, C.-W. Wu, Y.-H. Huang, H.-W. Song, C.-G. Huang, Interlaminar damage of carbon fiber reinforced polymer composite laminate under continuous wave laser irradiation, Opt. Lasers Eng. 88 (2017) 91–101.
[35] J. Panta, A.N. Rider, J. Wang, C.H. Yang, R.H. Stone, A.C. Taylor, N. Brack, S. Cheevers, Y.X. Zhang, High-performance carbon nanofiber reinforced epoxy-based nanocomposite adhesive materials modified with novel functionalization method and triblock copolymer, Compos. B Eng. 249 (2023) 110401.
[36] J. Panta, A.N. Rider, J. Wang, R.C. Yang, R.H. Stone, A.C. Taylor, S. Cheevers, A. L. Farnsworth, Y.X. Zhang, Influence of amino-functionalized carbon nanotubes and acrylic triblock copolymer on lap shear and butt joint strength of high viscosity epoxy at room and elevated temperatures, Int. J. Adhes. Adhes. 134 (2024) 103770.
[37] J. Li, C. Zhu, Z. Zhao, P. Khalili, M. Clement, J. Tong, X. Liu, X. Yi, Fire properties of carbon fiber reinforced polymer improved by coating nonwoven flame retardant mat for aerospace application, J. Appl. Polym. Sci. 136 (2019) 47801.
[38] R.D. Chippendale, I.O. Golosnoy, P.L. Lewin, Numerical modelling of thermal decomposition processes and associated damage in carbon fibre composites, J. Phys. D Appl. Phys. 47 (2014) 385301.
[39] N. Dellinger, G. Leplat, C. Huchette, V. Biasi, F. Feyel, Numerical modeling and experimental validation of heat and mass transfer within decomposing carbon fibers/epoxy resin composite laminates, Int. J. Therm. Sci. 201 (2024) 109040.
[40] A.P. Mouritz, S. Feih, E. Kandare, Z. Mathys, A.G. Gibson, P.E. Des Jardin, S. W. Case, B.Y. Lattimer, Review of fire structural modelling of polymer composites, Compos. A: Appl. Sci. Manuf. 40 (2009) 1800–1814.